CIVIL ENGINEERING JOURNAL

Article no. 30

THE CIVIL ENGINEERING JOURNAL 2-2021

TORSIONAL SHEAR STRESS WITH ARBITRARY CROSS-SECTIONS IN HOMOGENEOUS ISOTROPIC ELASTIC MATERIAL USING FINITE ELEMENT METHOD

Dang-Bao Tran[1,2]

1. *VSB–Technical University of Ostrava, Faculty of Civil Engineering, Department of Structures, Ludvíka Podéště 1875/17, 708 00 Ostrava, Czech Republic; dang.bao.tran@vsb.cz*
2. *Thu Dau Mot University, Faculty of Architecture, Department of Civil Engineering, Tran Van On 06, 75000 Binh Duong Province, Vietnam;baotd@tdmu.edu.vn*

ABSTRACT

Determining the shear stress of a structural element caused by torsion is a vital problem. The analytical solution of the Saint-Venant torsion is only suitable for simple cross-sections. The numerical methods to evaluate the shear stress due to torsion of complicated cross-sections is indispensable. Many scientists have studied the torsion problem with various numerical methods. This paper aims to present an efficient finite element method for assessing the shear stress with arbitrary cross-sections in homogeneous isotropic elastic material due to torsion. MATLAB is the language for programming the numerical method. The validation examples were performed to show the reliability and efficiency of the author's numerical method.

KEYWORDS

Torsional shear stress, Isoparametric eight-noded quadrilateral elements, Saint-Venant torsion, Warping function

INTRODUCTION

Torsion in the structure occurs due to asymmetrical loads, either by geometric dimensions or by interconnections between members. In many cases, torsion can be governing design factors. It is, therefore, essential to accurately determine the shear stress caused by torsion. Saint-Venant analysed the torsion problem using the semi-inverse method, assuming an unknown displacement to satisfy the equilibrium equations and boundary conditions. Prandtl then introduced the stress function of the Saint-Venant torsion and the method of membrane analogy [1]. However, determining the shear stress due to torsion by the analytic solution is complicated for a complex single connected domain or multiply connected domain. A single connected domain is a domain where the cross-section is bounded by a closed. The multiply connected domain is the domain where the cross-section is bordered by several closed.

Nowadays, structural elements such as beams and columns are more and more complicated in their shapes. Hence the use of numerical methods to determine shear stress due to torsion is indispensable. Various numerical methods to assess torsional shear stress have been performed by many researchers [2-22]. Ely, J. F., and Zienkiewicz, O. C. [2] first solved Poisson's equation of Prandtl's stress function using the finite difference method and investigated the rectangular section with and without holes. Herrmann, L. R. [3] utilized the finite element method to calculate the warping function of the torsion of irregular sectional shapes. Based on the Hellinger–Reissner principle, Xiao, Q. Z., et al. [4] developed a 4-node element with four stress parameters to determine the shear

stress for the polygonal section. Gruttmann, F. et al. [5] used the finite element method to evaluate shear stress using the warping function, which is more convenient than using Prandtl's stress function when considering a multiply connected domain. Gruttmann's numerical method has been implemented into an enhanced version of the program FEAP [6], which used isoparametric four-noded quadrilateral elements. Fialko, S.Y. et al. [7] developed a numerical method using constant triangular elements to solve the Saint Venant problem of torsion, and torsionless bending of prismatic bars is realized in the SCAD software [8]. Jog, S. et al. [9] presented a finite-element formulation for Saint Venant torsion with a multiply-connected domain in an anisotropic material. Recently, Beheshti, A. [10] derived a finite element from strain-gradient elasticity for torsion of prismatic bars with minimal dimensions.

Besides the finite difference and finite element method, many authors have applied other numerical methods such as the boundary element method (BEM) [11-16], line element-less method (LEM) [17-18], a null-field integral technique [19], and finite-volume method [20-21] to analyse the torsion problem. Katsikadelis, J. T. et al. [11] examined the torsion of general composite bars by BEM while Gaspari, D. et al. [12] tackled orthotropic beams with a polygonal cross-section. Barone, G. et al. [13] implemented the Complex Variable Boundary Element Method to examine the torsion problem in the single connected domain. Lee, J.W. et al. [14] obtained a new BEM from the general Cauchy integral formula derived from the Borel–Pompeiu formula to analyse the torsion problem. Paradiso, M. et al. [15] achieved an efficient method to determine the warping function parameter with the general cross-section. Chen, K. H. et al. [16] introduced a new error estimation technique in BEM to optimise the torsion problem with a multiply-connected domain. Di Paola, M. et al. [17] proposed LEM to deal with shear stress in torsion problem with isotropic material and arbitrary cross-section. Santoro, R. [18] handled the Saint Venant torsion problem for orthotropic beams with a general cross-section by LEM. Chen, J-T. et al. [19] introduced the null-field integral technique to analyse the torsion problem of circular cross-sections with round holes. Chen, H. et al. [20-21] developed a new finite-volume based on Bansal and Pindera's work to investigate Saint Venant's torsion problems of homogeneous and composite prismatic bars with multiply connected domain.

In summary, all of the works show the feasibility and effectiveness in academia. Currently, to the author's knowledge, Gruttmann's method [5] has been developed into the FEAP program [6] of the University of California, Berkeley, and Allplan Bridge [22]. Fialko's method [7] is similar to Gruttmann, developed as a module in the SCAD commercial software [8]. It means the methods of Gruttmann and Fialko are practical. However, due to the use of the four-noded quadrilateral element in FEAP and the constant strain triangle element in SCAD, to achieve high accuracy, it is necessary to mesh very smoothly, which affects the calculation speed. So, this research aims to develop a new numerical method (NMB) based on the work of Gruttmann by using the isoparametric eight-noded quadrilateral element. The validation examples were performed to show the reliability and efficiency of NMB.

FINITE ELEMENT METHOD PROCEDURE

Figure 1 shows the arbitrary cross-section of prismatic beam in homogeneous isotropic elastic material, the longitudinal axis is the x-axis, the cross-section denoted Ω is in yz plane. The multiply connected domain Ω is bounded by Γ_1, Γ_2,..., Γ_{n-1}, Γ_n . S is the centre of gravity. On Γ_1, Γ_2,..., Γ_{n-1}, Γ_n the right-handed orthogonal basis system is defined with tangent vector **t** and outward normal vector $\mathbf{n}=[n_y, n_z]^T$. With **t** the orientation of the associated coordinate *s* is uniquely defined.

The displacement field $\mathbf{u}=[\mathrm{u_x}, \mathrm{u_y}, \mathrm{u_z}]^T$ is expressed as [1]

$$u_x = \alpha\omega^T, u_y = -\beta_x z, \; u_z = -\beta_x y, \tag{1}$$

where β_x: torsion angle, $\alpha = \frac{d\beta_x}{dx}$, $\omega^T(y,z)$: warping function for torsion. Here, the constraint of the warping for torsion is

$$\int_{\Omega} \omega^T dA = 0. \tag{2}$$

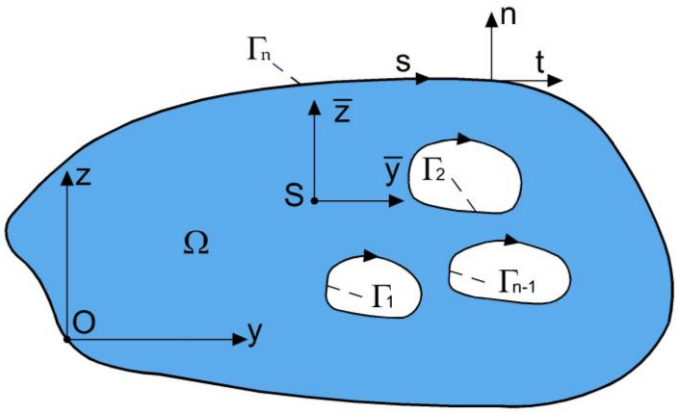

Fig. 1 - Cross-section of a prismatic bar.

The shear stresses are given as

$$\tau_{xy} = G\alpha\left(\frac{\partial\omega^T}{\partial y} - z\right),\ \tau_{xz} = G\alpha\left(\frac{\partial\omega^T}{\partial z} + y\right). \tag{3}$$

The polar second moment of area can be written as

$$I_T = \int_{\Omega}\left[\left(\frac{\partial\omega^T}{\partial z} + y\right)y - \left(\frac{\partial\omega^T}{\partial y} - z\right)z\right]dA. \tag{4}$$

The governing differential equation for the Saint-Venant torsion is expressed as

$$\frac{\partial^2\omega^T}{\partial^2 y} + \frac{\partial^2\omega^T}{\partial^2 z} = 0 \quad in\ \Omega. \tag{5}$$

Meanwhile, the boundary condition is given as

$$n_y\frac{\partial\omega^T}{\partial y} + n_z\frac{\partial\omega^T}{\partial z} = n_y z - n_z y \quad on\ \Gamma_i (i = 1,2,...,n), \tag{6}$$

$$\text{where } n_y = \frac{dz}{ds},\ n_z = -\frac{dy}{ds}. \tag{7}$$

The governing differential equation (5) is transformed into the weak form by using the Galerkin's method as below

$$G(\omega^T,\eta) = \int_{\Omega}\left[\frac{\partial\omega^T}{\partial y}\frac{\partial\eta}{\partial y} + \frac{\partial\omega^T}{\partial z}\frac{\partial\eta}{\partial z}\right]dA - \oint_{\partial\Omega}(n_y z - n_z y)\eta ds = 0, \tag{8}$$

with test function $\eta \in H^1(\Omega)$.

The equation (8) is approximated by using the finite element method. Gruttmann's method used isoparametric four-noded quadrilateral elements. To improve the computation speed, NMB used isoparametric eight-noded quadrilateral elements. The $\mathbf{x}=[y,z]^T$, the unknown function ω^T and the test function η are interpolated in the local coordinate system as follows

$$\mathbf{x}^h=\sum_{i=1}^{8}N_i(\xi,\eta)\mathbf{x}_i\ ,\ (\omega^T)^h=\sum_{i=1}^{8}N_i(\xi,\eta)\omega_i^T\ ,\ (\eta)^h=\sum_{i=1}^{8}N_i(\xi,\eta)\eta_i, \tag{9}$$

where *h* denotes the approximate solution of the finite element method, $N_i(\xi,\eta)$ denotes the shape function of the element. Figure 2 shows the isoparametric eight-noded quadrilateral element used in NMB. The shape functions of this element can be described as follows [23, 24]

$$\begin{aligned}
N_1(x,h)&=\frac{1}{4}(1-x)(1-h)(-1-x-h),\ N_2(x,h)=\frac{1}{4}(1+x)(1-h)(-1+x-h),\\
N_3(x,h)&=\frac{1}{4}(1+x)(1-h)(-1+x+h),\ N_4(x,h)=\frac{1}{4}(1-x)(1+h)(-1+x+h),\\
N_5(x,h)&=\frac{1}{2}(1-x^2)(1-h),\ N_6(x,h)=\frac{1}{2}(1+x)(1-h^2),\\
N_7(x,h)&=\frac{1}{2}(1-x^2)(1+h),\ N_8(x,h)=\frac{1}{2}(1-x)(1-h^2).
\end{aligned} \tag{10}$$

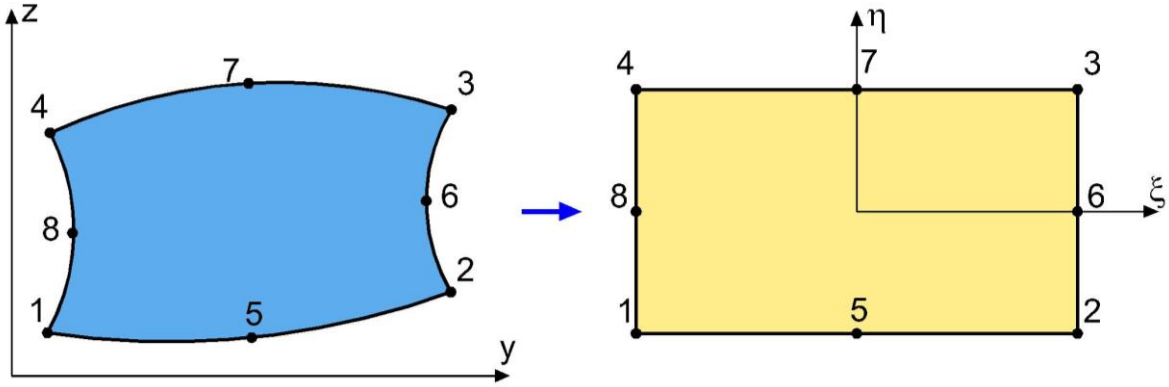

Fig 2 -. Isoparametric eight-noded quadrilateral element.

Inserting the derivatives of $(\omega^T)^h$ and η^h into the equation (8) reads as

$$\bigcup_{e=1}^{numel}\sum_{i=1}^{8}\sum_{j=1}^{8}(K_{ij}^e\omega_j^T-F_i^e)=0. \tag{11}$$

Here, $\bigcup$ denotes the assembly operator with *numel* the total number finite elements. The stiffness part K_{ij}^e to the nodes *i* and *j* and the right hand F_i^e read

$$\begin{aligned}
K_{ij}^e&=\int_{\Omega_e}\left(\frac{\partial N_i}{\partial y}\frac{\partial N_j}{\partial y}+\frac{\partial N_i}{\partial z}\frac{\partial N_j}{\partial z}\right)dA_e=\int_{-1}^{1}\int_{-1}^{1}\left(\frac{\partial N_i}{\partial y}\frac{\partial N_j}{\partial y}+\frac{\partial N_i}{\partial z}\frac{\partial N_j}{\partial z}\right)|\mathbf{J}|d\xi d\eta,\\
K_{ij}^e&=\sum_{p=1}^{P}\sum_{q=1}^{Q}w_pw_q\left(\frac{\partial N_i}{\partial y}(\xi_p,\eta_q)\frac{\partial N_j}{\partial y}(\xi_p,\eta_q)+\frac{\partial N_i}{\partial z}(\xi_p,\eta_q)\frac{\partial N_j}{\partial z}(\xi_p,\eta_q)\right)\left|\mathbf{J}(\xi_p,\eta_q)\right|.
\end{aligned} \tag{12}$$

$$F_i^e = \int_{\Omega_e} \left(\frac{\partial N_i}{\partial y} z - \frac{\partial N_i}{\partial z} y \right) dA_e = \int_{-1}^{1} \int_{-1}^{1} \left(\frac{\partial N_i}{\partial y} z - \frac{\partial N_i}{\partial z} y \right) |\mathbf{J}| d\xi d\eta,$$
$$F_i^e = \sum_{p=1}^{P} \sum_{q=1}^{Q} w_p w_q \left(\frac{\partial N_i}{\partial y}(\xi_p, \eta_q) z - \frac{\partial N_i}{\partial z}(\xi_p, \eta_q) y \right) |\mathbf{J}(\xi_p, \eta_q)|. \quad (13)$$

where $\mathbf{J}$ denoted as Jacobian matrix defined as

$$\mathbf{J} = \begin{bmatrix} \frac{\partial y}{\partial x} & \frac{\partial z}{\partial x} \\ \frac{\partial y}{\partial h} & \frac{\partial z}{\partial h} \end{bmatrix} \quad (14)$$

w_p and w_q are the weights and ξ_p and η_q are the integration points of the Gaussian integration technique. NMB uses 3 x 3 Gauss quadrature derived from the 1D case, where the quadrature points are located at $-\sqrt{3/5}$, 0 and $\sqrt{3/5}$, and the corresponding weights are equal to 5/9, 8/9, and 5/9, respectively (see [23, 24]). The value ω_i^T of one arbitrary nodal point *i* has to be value 0.

VALIDATION EXAMPLES

The objective of this section is to demonstrate the reliability and effectiveness of NMB. For this purpose, four validation examples derived from [1, 5, 9] were examined, and their results are compared with those analyzed by NMB implemented in MATLAB R2015a.

A bar of square cross-section subjected to the torsion moment $M_T = 1$ kN.m with the length of the edge 2 m is analysed in the first example. Jog, C.S. et al. [9] investigated this problem using 16 isoparametric nine-noded quadrilateral elements. To achieve convergence values of the shear stress and the polar second moment of area, the square cross-section is divided into 16, 64, 256 elements with uniform mesh by NMB, respectively. Figure 3 shows the discretization of the square cross-section with 16 eight-noded quadrilateral elements. The points, A, B, C, D, correspond with the coordinates (0, 1), (2, 1), (0, 0), (0, 2), respectively.

The analytical results of maximum shear stress and polar second moment of area obtained from [1, 9] are $\tau_{\max} = 0.592$ kPa, $I_T = 2.24923$ m^4, respectively. Table 1 shows the comparison of the results of the maximum shear stress, the polar second moment of area between the methods. The results of NMB-16 elements and Jog, C.S. et al. [9] are the same. When the square cross-section is refined into 256 elements, NMB is in good agreement with analytical solutions.

Tab. 1 - The maximum shear stress $\tau_{\max}$ and the polar second moment of area I_T of square cross-section

Factors	Analytical solutions	Jog, C.S. et al. [9]	NMB- 16 elements	NMB- 256 elements
$\tau_{\max}^{(a)}$ [kPa]	0.592	0.6173	0.619174	0.601461
$I_T^{(b)}$ [m^4]	2.24923	2.2519	2.25187	2.24925
Error$^{(a)}$, (%)	-	4.273	4.590	1.598
Error$^{(b)}$, (%)	-	0.1187	0.1173	0.000

Figure 4 depicts the distribution of shear stress τ_{xz} for square cross-section, which decreases the magnitude gradually from the midpoint of the edge to the centre of gravity along the y-axis [1].

Figure 5 and 6 present the variation of the shear stress τ_{xz} along the AB and CD segment, respectively. With 16 elements, NMB and Jog, C.S. et al. [9] cannot capture precisely the shear stress distribution along the CD segment. When the mesh is fine enough, in this case, 256 elements, the results of NMB and theory harmonize very well.

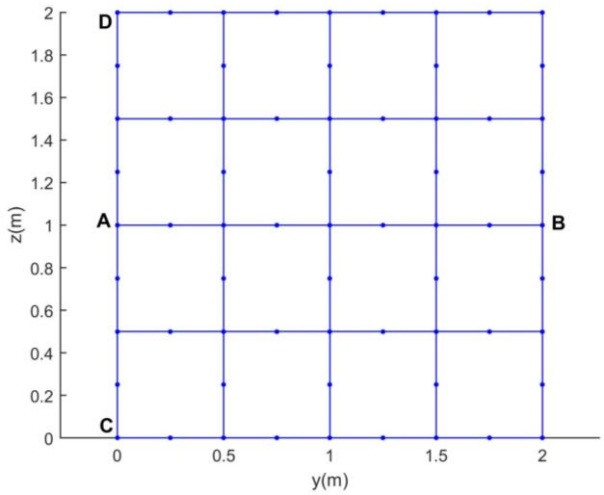

Fig. 3 - Discretization of the square cross-section with 16 elements.

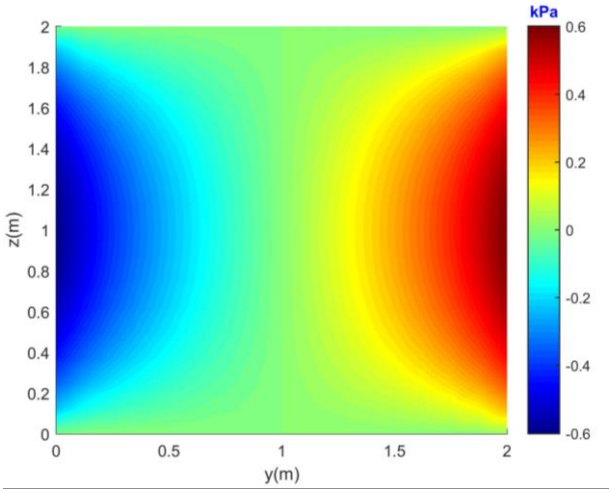

Fig. 4 - Distributed shear stresses τ_{xz} for square cross-section.

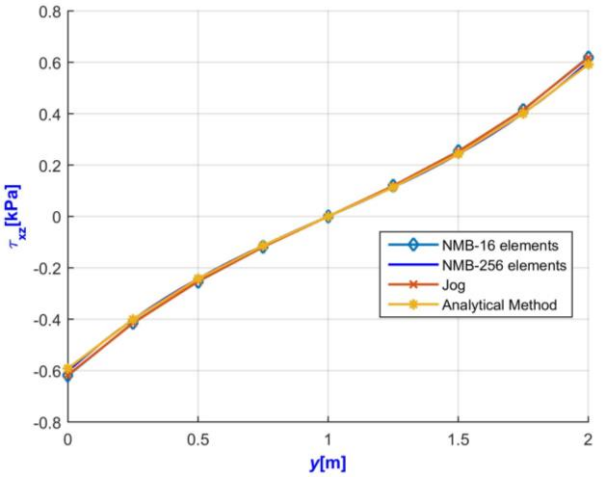

Fig. 5 - The variation of shear stress τ_{xz} along the AB segment.

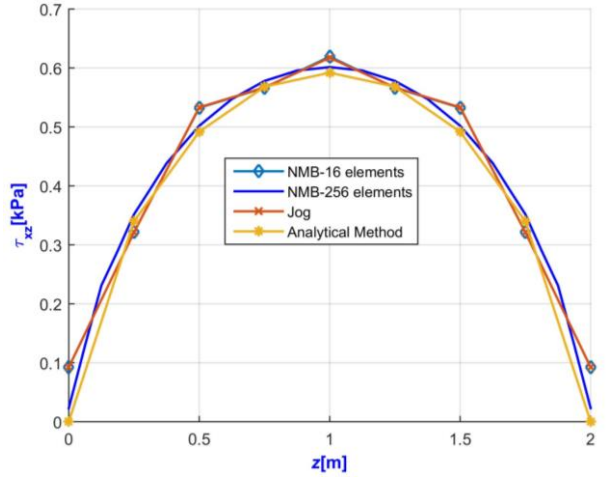

Fig. 6 - The variation of shear stress τ_{xz} along the CD segment.

The second example is an equilateral triangle subjected to the torsion moment $M_T = 1$ kN.m with the height of the triangle 0.2 m. The analytical results of maximum shear stress $\tau_{\max}$ and polar second moment of area I_T are 1.62380 MPa and 6158.40 cm^4, respectively [1]. The triangular cross-section was discretized 4, 8, 14, 37, 57, 109, 658 eight-noded quadrilateral elements with non-uniform mesh to obtain the convergence results.

Tab. 2 - The maximum shear stress τ_{max} and the polar second moment of area I_T of triangular cross- section

Factors	Analytical solution	NMB- 658 elements	Error, (%)
τ_{max} [MPa]	1.62380	1.6247	0.055
I_T [cm^4]	6158.40	6158.40	0.000

It is clear from Table 2 that the results of the maximum shear stress, the polar second moment of area obtained from NMB are in good agreement with the theoretical solution [1]. Figure 7 shows the triangular cross-section divided by 14 eight-noded quadrilateral elements. The points, E, F, correspond with the coordinates (0, $\frac{0.2}{\sqrt{3}}$), (0.2, $\frac{0.2}{\sqrt{3}}$), respectively.

Figure 8 depicts the stress distribution τ_{xy} for triangular cross-section, where magnitude values do not exist along with segment EF [1]. Figure 9 presents the stress distribution τ_{xz} for triangular cross-section. It can observe from Figure 10 that the result of the variation of shear stress τ_{xz} along the EF segments of NMB and analytical method is very well matched.

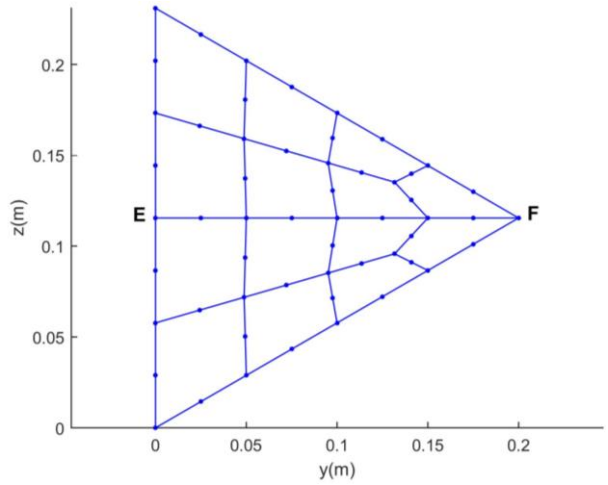

Fig. 7 - Discretization of the triangular cross-section with 14 elements.

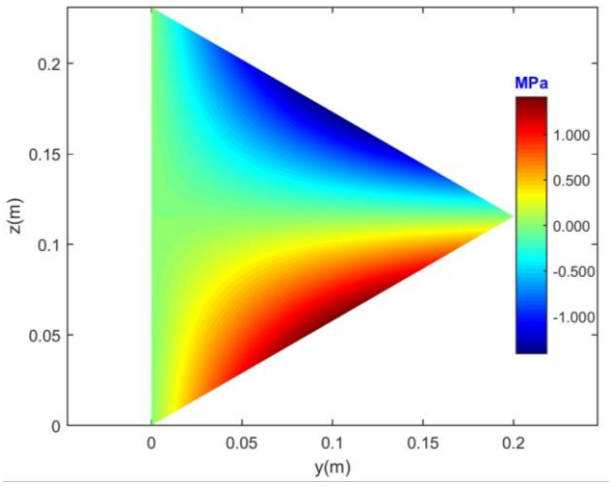

Fig. 8 - Distributed shear stresses τ_{xy} for triangular cross-section.

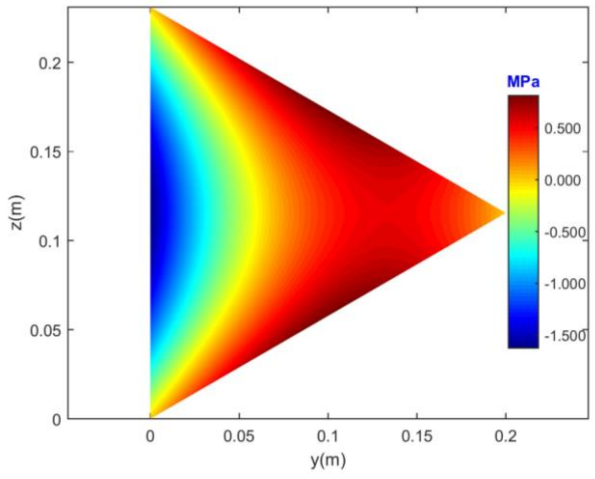

Fig. 9 - Distributed shear stresses τ_{xz} for triangular cross-section.

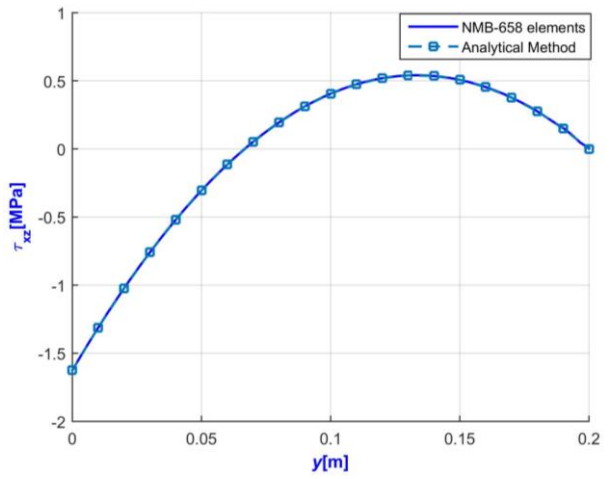

Fig. 10 - The variation of shear stress τ_{xz} along the EF segment with NMB-109 element.

The third example concerns a bar of square cross-section with hole applied to the torsion moment $M_T = 1$ kN.m. Figure 11 shows the geometrical dimensions and the meshing to 96 isoparametric eight-noded quadrilateral elements by NMB of the square cross-section with hole. The points, G, H, I, J, correspond with the coordinates (0, 1), (1.6, 1), (0, 0), (0, 2), respectively.

Jog, C.S. et al. [9] analysed this problem using 96, 1536, 6144 isoparametric nine-noded quadrilateral elements, respectively. Figure 12 depicts the variation of polar second moment of area corresponding to 96, 1536, 6144 discretization elements investigated by NMB. In Table 3, the convergence of the polar second moment of area value by NMB is presented as a comparison with that obtained from Jog, C.S. et al. [9]. Figure 13 and 14 present the stress distribution τ_{xy}, τ_{xz} for square cross-section with hole, respectively. Figure 15 and 16 plot the variation of shear stress τ_{xz} along the segments, GH, IJ, respectively, evaluated with the two methods, Jog, C.S. et al. [9], and NMB. From the figures and table mentioned above, the reliability of the NMB is once more verified.

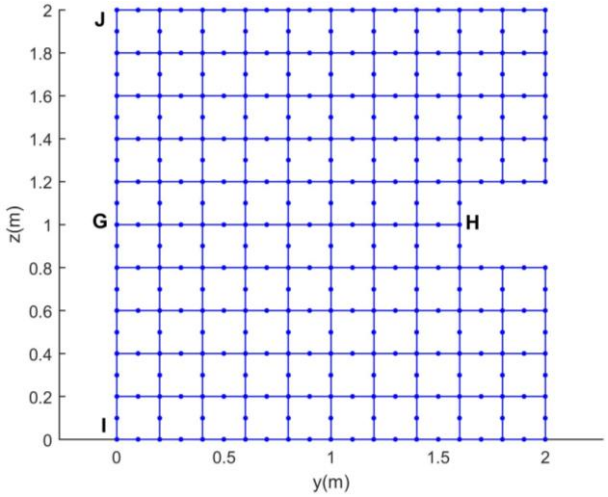

Fig. 11 - The dimension and the discretization to 96 elements of the square cross-section with hole.

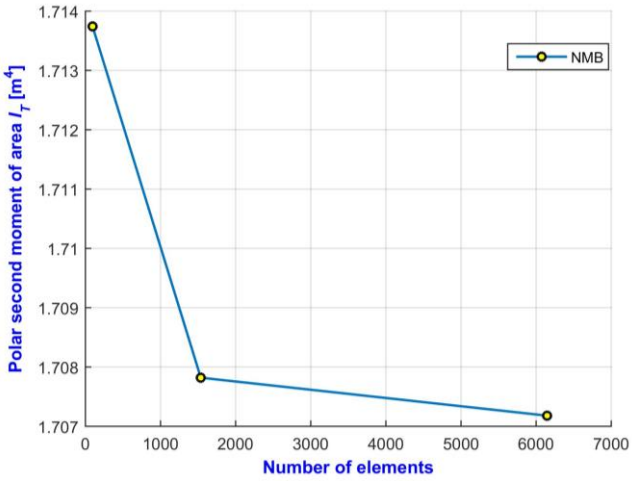

Fig. 12 - The variation of polar second moment of area corresponding to discretization elements.

Tab. 3 - The polar second moment of area of square cross-section with hole

Factors	Jog, C.S. et al.- 6144 elements [9]	NMB- 6144 elements	Error, (%)
I_T [m^4]	1.707	1.70718	0.01054

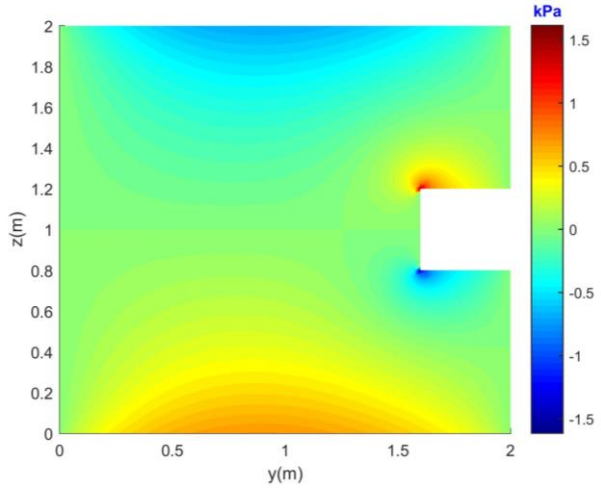

Fig. 13 - Distributed shear stresses τ_{xy} for the square cross-section with hole.

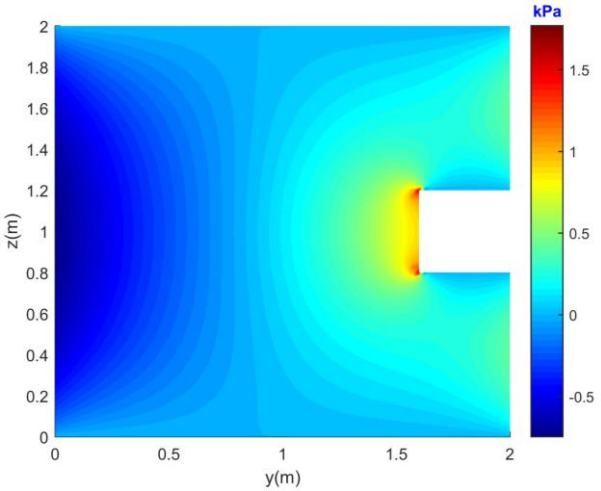

Fig. 14 - Distributed shear stresses τ_{xz} for the square cross-section with hole.

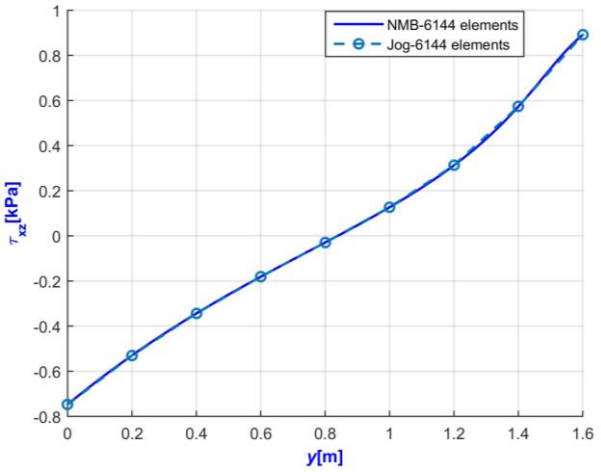

Fig. 15 - The variation of shear stress τ_{xz} along the GH segment.

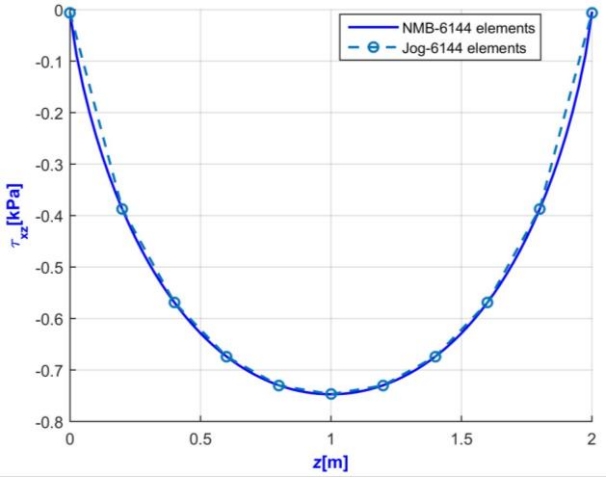

Fig. 16 - The variation of shear stress τ_{xz} along the IJ segment.

According to Figure 17, the bridge cross-section is an example for multiply connected domains was considered the fourth example. With this example, the polar second moment of area of the bridge cross-sections neglected the cantilever part obtained by the analytical solution is 40.0 m^4 [5]. A comparison with a theoretical explanation is not possible. The comparison between NMB and FEAP [5,6], implemented Gruttmann's numerical method by using isoparametric four-noded quadrilateral element, was performed on the convergence speed. The bridge cross-section was divided into 50000 nodes with a uniform mesh by FEAP to obtain the convergence of the results.

In NMB, the bridge cross-section is meshed with 80, 406, 1892, 4634, 11414 nodes to investigate the convergence result. Figure 18 shows the bridge cross-section divided into 80 nodes by NMB. Figure 19 depicts the convergence of the polar second moment of area obtained by NMB with 4634 nodes.

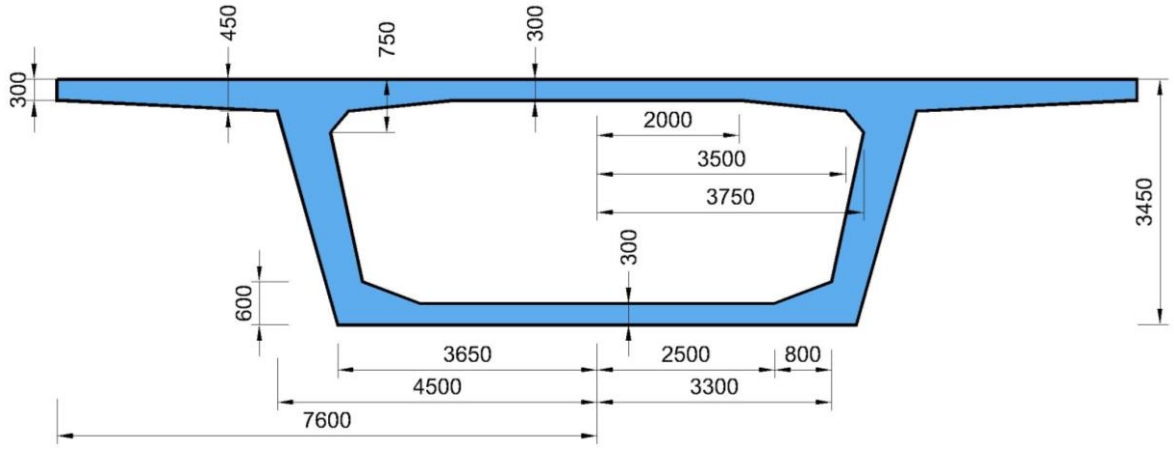

Fig. 17 - Bridge cross-section, with measurements in [m].

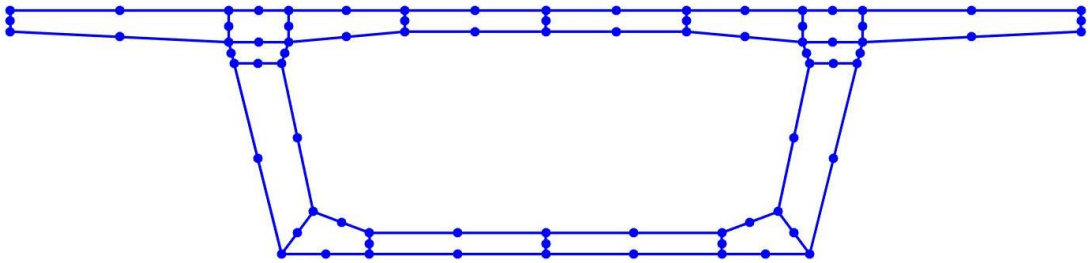

Fig.18 - Discretization of the bridge cross-section to 80 nodes by NMB.

The comparison of the polar second moment of area between the two methods was performed. In Table 4, we can see that the error of the value of the polar second moment of area between the two methods is 1.904%. It should be emphasized that there is no exact analytical solution for this example, and the number of nodes required for the convergence problem of NMB is 10.8 times smaller than that of FEAP. From Table 4, the efficiency of NMB is verified. Figure 20 shows the shear flow of the bridge cross-section under torsion $M_T = 1$ kN.m of NMB. As expected, shear stress is mainly concentrated in the closed part of the section [5].

Tab. 4 - The polar second moment of area of bridge cross-section

Factors	FEAP- 50000 nodes [5,6]	NMB- 4634 nodes	Error, (%)
I_T [m^4]	42.487	43.2963	1.904

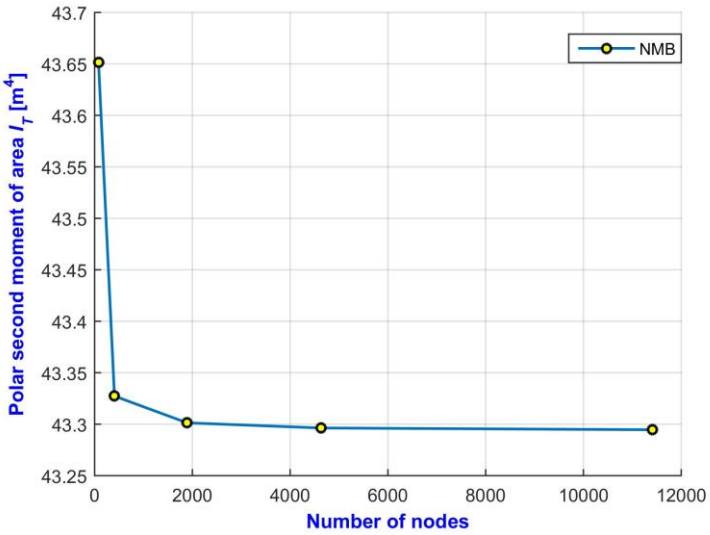

Fig.19 - The values of polar second moment of area with respect to the number of nodes in bridge cross-section.

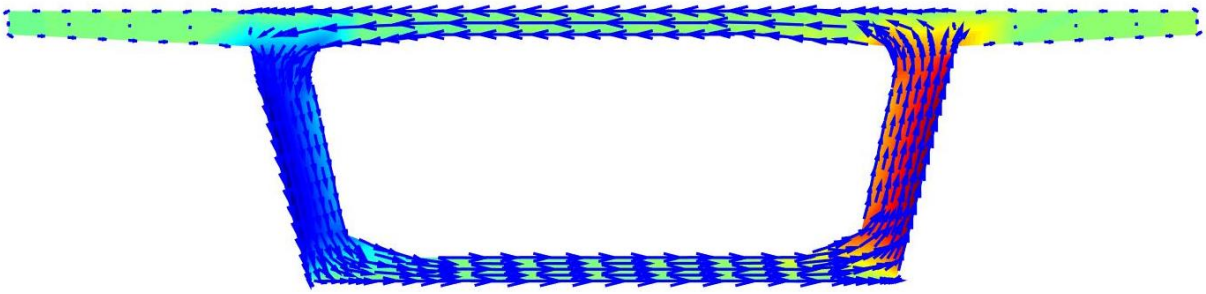

Fig.20.- Shear flow for the bridge cross-section under torsion of NMB.

CONCLUSION

Gruttmann [5] proposed an excellent finite element method for evaluating shear stress due to torsion with arbitrary cross-sections in homogeneous isotropic elastic material based on the Saint-Venant theory. However, the use of isoparametric four-noded quadrialeral elements made the method not reach the best optimization. NMB has been improved Gruttmann's work by using isoparametric eight-noded quadrilateral elements. Through 4 validated examples represented by single connected domain and multiply connected domains, it can conclude that NMB is reliable and efficient in assessing shear stress due to torsion. The shear stress research due to torsion of the arbitrary reinforced concrete section is desirable in the future.

ACKNOWLEDGEMENTS

The works were supported from the Student Grant Competition VSB-TUO. The registration number of the project is SP2021/77 "Nonuniform torsion in prismatic beams with arbitrary cross-sections using FEM".

REFERENCES

[1] Timoshenko, S., Goodier, J. N. Theory of Elasticity, by S. Timoshenko and JN Goodier,... McGraw-Hill book Company, 1951.
[2] Ely, J. F., and Zienkiewicz, O.C. "Torsion of compound bars—A relaxation solution." *International Journal of Mechanical Sciences* 1.4 (1960): 356-365.
[3] Herrmann, L.R. "Elastic torsional analysis of irregular shapes." *Journal of the Engineering Mechanics Division* 91.6 (1965): 11-19.
[4] Xiao, Q. Z., et al. "An improved hybrid-stress element approach to torsion of shafts." *Computers & structures* 71.5 (1999): 535-563.
[5] Gruttmann, F., Sauer, R. and Wagner, W. "Shear stresses in prismatic beams with arbitrary cross-sections." *International journal for numerical methods in engineering* 45.7 (1999): 865-889.
[6] 2021. Available online: http://projects.ce.berkeley.edu/feap/ (accessed on 08 June 2021).
[7] Fialko, S.Y. and Lumelskyy, D.E. "On numerical realization of the problem of torsion and bending of prismatic bars of arbitrary cross section." *Journal of Mathematical Sciences* 192.6 (2013): 664-681.
[8] Scadsoft. Available online: https://scadsoft.com/en (accessed on 08 June 2021).
[9] Jog, C.S. and Mokashi, I.S. "A finite element method for the Saint-Venant torsion and bending problems for prismatic beams." *Computers & Structures* 135 (2014): 62-72.
[10] Beheshti, A. "A numerical analysis of Saint-Venant torsion in strain-gradient bars." *European Journal of Mechanics-A/Solids* 70 (2018): 181-190.
[11] Katsikadelis, J.T. and Sapountzakis, E.J. "Torsion of composite bars by boundary element method." *Journal of engineering mechanics* 111.9 (1985): 1197-1210.
[12] Gaspari, D. and Aristodemo, M. "Torsion and flexure analysis of orthotropic beams by a boundary element model." *Engineering analysis with boundary elements* 29.9 (2005): 850-858.
[13] Barone, G., Iacono, F.L. and Navarra, G. "Complex potential by hydrodynamic analogy for the determination of flexure–torsion induced stresses in De Saint Venant beams with boundary singularities." *Engineering Analysis with Boundary Elements* 37.12 (2013): 1632-1641.
[14] Lee, J.W., Hong, H.K. and Chen, J.T., "Generalized complex variable boundary integral equation for stress fields and torsional rigidity in torsion problems." *Engineering Analysis with Boundary Elements* 54 (2015): 86-96.
[15] Paradiso, M., et al. "A BEM approach to the evaluation of warping functions in the Saint Venant theory." *Engineering Analysis with Boundary Elements* 113 (2020): 359-371.
[16] Chen, K. H., et al. "A new error estimation technique for solving torsion bar problem with inclusion by using BEM." *Engineering Analysis with Boundary Elements* 115 (2020): 168-211.
[17] Chen, J.T. and Lee, Y.T. "Torsional rigidity of a circular bar with multiple circular inclusions using the null-field integral approach." *Computational Mechanics* 44.2 (2009): 221-232.
[18] Di Paola, M., Pirrotta, A. and Santoro, R. "Line element-less method (LEM) for beam torsion solution (truly no-mesh method)." *Acta Mechanica* 195.1 (2008): 349-364.
[19] Santoro, R. "The line element-less method analysis of orthotropic beam for the De Saint Venant torsion problem." *International journal of mechanical sciences* 52.1 (2010): 43-55.
[20] Chen, H., Gomez, J. and Pindera, M.J. "Saint Venant's torsion of homogeneous and composite bars by the finite volume method." *Composite Structures* 242 (2020): 112128.
[21] Chen, H., Gomez, J. and Pindera, M.J. "Parametric finite-volume method for Saint Venant's torsion of arbitrarily shaped cross sections." *Composite Structures* 256 (2021): 113052.
[22] Allplan Bridge Features. Available online: https://www.allplan.com/products/allplan-bridge-2019-features/ (accessed on 08 June 2021).
[23] Zienkiewicz, O.C., Taylor, R.L. and Zhu, J.Z. *The finite element method: its basis and fundamentals. Elsevier*, 2005.
[24] Bathe, K.J. "Finite Element Procedures Prentice-Hall." *New Jersey* 1037 (1996).